HHS Public Access

Author manuscript

Nature. Author manuscript; available in PMC 2014 January 04.

Published in final edited form as:

Nature. 2013 July 4; 499(7456): 107–110. doi:10.1038/nature12233.

Structural Basis for Alternating Access of a Eukaryotic Calcium/Proton Exchanger

Andrew B. Waight[1], **Bjørn Panyella Pedersen**[1], **Avner Schlessinger**[2], **Massimiliano Bonomi**[2], **Bryant H. Chau**[1], **Zygy Roe-Zurz**[1], **Aaron J. Risenmay**[1], **Andrej Sali**[2], and **Robert M. Stroud**[1]

[1] Department of Biochemistry and Biophysics, University of California, San Francisco, CA 94158, United States of America.

[2] Department of Bioengineering and Therapeutic Sciences, Department of Pharmaceutical Chemistry, California Institute for Quantitative Biosciences, University of California, San Francisco, CA 94158, United States of America.

Eukaryotic Ca^{2+} regulation involves sequestration into intracellular organelles, and expeditious Ca^{2+} release into the cytosol is a hallmark of key signaling transduction pathways. Bulk removal of Ca^{2+} following such signaling events is accomplished by members of the Ca^{2+}:cation (CaCA) superfamily[1–5]. The CaCA superfamily includes the Na^{+}/Ca^{2+} (NCX) and Ca^{2+}/H^{+}(CAX) antiporters, and in mammals the NCX and related proteins constitute families SLC8 and SLC24, and are responsible for the re-establishment of Ca^{2+} resting potential in muscle cells, neuronal signaling and Ca^{2+} reabsorption in the kidney[1,6]. The CAX family members maintain cytosolic Ca^{2+} homeostasis in plants and fungi during steep rises in intracellular Ca^{2+} due to environmental changes, or following signal transduction caused by events such as hyperosmotic shock, hormone response and response to mating pheromones[7–13]. The cytosol-facing conformations within the CaCA superfamily are unknown, and the transport mechanism remains speculative. We determined a crystal structure of the *Saccharomyces cerevisiae* vacuolar $Ca^{2+/}H^{+}$ exchanger (VCX1) at 2.3Å resolution in a cytosol-facing, substrate bound conformation. VCX1 is the first structure within the CAX family, and it describes the key cytosol-facing conformation of the CaCA superfamily, providing the structural basis for a novel alternating access mechanism

Correspondence and requests for materials should be addressed to R.M.S. (stroud@msg.ucsf.edu)..

Author Contributions

A.B.W. optimized the yeast expression system, performed expression, purification and crystallization experiments, collected and processed the data, determined, refined and analysed the structure, and performed reconstitution and transport assays. B.P.P. performed data collection and assisted with structure solution and structural analysis. B.C. and A.R. assisted in cell harvesting, membrane preparation and purification experiments. B.C. and Z. R-Z. did cloning and expression tests. A.Sc. constructed VCX1 comparative models as well as performed bioinformatics and distance plot analysis. M.B. performed molecular dynamics simulations and distance plot analysis. A.B.W., B.P.P., and R.M.S. wrote the paper with input from A.Sc, M.B. and A.S.

Competing financial interests

The authors declare no competing financial interests

Author Information

Coordinates and structure factors have been deposited in the Protein Data Bank with the accession number 4K1C.

by which the CaCA superfamily performs high-throughput Ca^{2+} transport across membranes.

The CaCA superfamily is defined by the presence of two short, repeating homologous sequences, termed the α-repeats, found in predicted transmembrane regions. The α-repeats are opposite in topology and are believed to have arisen from a gene duplication event[14–16]. Mutagenesis and recent structural data have identified this region as essential for ion binding and transport, and specifically two key acidic residues (Glu or Asp) are implicated in coordinating Ca^{2+} ions at the active site[17–20]. Members of the CAX family are approximately 400 residues long with 11 predicted transmembrane helices. The first helix (MR), found in eukaryotic CAX members plays a regulatory role in plant members and is suggested to be involved in protein targeting and/or signaling in yeast[12,21,22]. The 10 remaining transmembrane helices (M1-M10) perform the transport function, and are composed of two symmetrically related halves (M1-M5 and M6-M10) connected through a negatively charged loop termed the "acidic motif"[12,16,23]. *S. cerevisiae* VCX1 catalyzes low affinity (K_m = ~25μM), high capacity (Vmax = ~35nmol Ca^{2+} min^{-1} mg^{-1}) vacuolar Ca^{2+} exchange[3,8,24,25]. To establish function of the purified protein, VCX1 was reconstituted into liposomes and assayed for Ca^{2+} uptake activity. In this system, purified VCX1 demonstrates Ca^{2+} uptake monotonically dependent on pH gradient (Supplementary Fig.1). VCX1 shares ~30% sequence identity with other members of the Ca^{2+}/H^+ exchanger family, including the canonical CAX proteins of *A. thaliana* (Supplementary Fig. 2).

VCX1 was solved experimentally to 2.3Å resolution (Rfree 22.4%) by molecular replacement, supported by iodine-based experimental phases (Fig. 1, Supplementary Table 1, Supplementary Fig 3). The structure encompasses residues 22-401 with the exception of a short loop (184-191) between M4 and M5. Two identical (RMSD 0.21Å over 285 Cα atoms) monomers are found in the asymmetric unit. Six divalent cations are identified as Ca^{2+} or Mn^{2+} in the VCX1 monomer, based on their coordination geometry and anomalous scattering differences (Supplementary Fig. 4).

The shape of the VCX monomer, viewed perpendicular to the membrane plane, resembles that of a wedge (Fig. 1). Viewed from the vacuolar side of the membrane, the tapered end of the wedge consists of two long anti-parallel helices M1 and M6, which are intertwined and tilted ~30° with respect to the membrane normal. The central four-helix core contains the α-repeats, and is comprised of M2-M3 and M7-M8. M2 and M7 are kinked at their midpoints and change direction ~35° in the middle of the membrane plane to create M2a/M2b and M7a/M7b. These two oppositely related helix kinks meet in the mid-membrane plane, forming an hourglass shape, where the CAX family display the conserved GNxxE(H) signature sequence necessary for calcium binding and transport[19,20,26,27]. M3 and M8 are also tilted with respect to the membrane normal and line the interior of the hourglass. M4-M5 and M9-M10 form the outer components of a right-handed bundle which flank the central core and constitute the thicker side of the wedge shape. The 20 residue "acidic motif" connecting the two duplicated halves of the protein between M5 and M6 is predicted to be disordered based on sequence. However, a clearly resolved α-helix (we term the Acidic Helix) for this sequence is observed in the structure. This helix is oriented parallel to the membrane and lies directly underneath the α-repeat regions on the cytosolic side.

A centrally located Ca^{2+} ion occupies the active site of VCX1, coordinated by Glu302 on M7b and Ser325 on M8 (Fig. 2). The Ser325 residue is generally conserved throughout the CaCA superfamily, and in NCX and NCKX family members the analogous serine residue has been shown to play an important role in Ca^{2+} transport (Supplementary Fig. 5)[18,19]. Three ordered water molecules complete the octahedral coordination geometry of Ca^{2+} (Supplementary Fig. 4b). The presence of water molecules at the binding site suggest that the Ca^{2+} ion reaches the active site in a partially hydrated state, balancing the stronger binding of entropically ordered side chains, with more loosely bound water to complete the coordination sphere. Glu106, Asn299 and the backbone carbonyl of Gly102 coordinate the three water molecules. The remainder of the Ca^{2+} active site is stabilized by specific interactions from polar residues in the transmembrane regions of M2, M3, M7, and M8. The conserved Asn299 and His303 of M7b form a hydrogen bond to Ser129 and Ser132 respectively, of the adjacent M3 helix, and the conserved Asn103 on M2b is hydrogen bonded to Gln328 on M8. M2a is bent away from the bundle of helices M2b, M3, M7 and M8, and in this configuration it is not packed tightly against the protein body (Fig. 3). M2a and the connected C-terminal half of M1 are bent away from the active site, exposing the central Ca^{2+} ion to the cytosol. The M2a/M1 arrangement creates a substantial vestibule that is accessible from the intracellular bulk solvent. This vestibule is conical in shape and has a negatively charged interior surface potential (Fig. 3c). The interior of the cavity vestibule is circumscribed by M2a, the C-terminal half of M1, M7b and the N-terminal half of M8, and allows access from the cytosol to the central Ca^{2+} binding site. Thus the VCX1 protein structure represents a substrate bound, cytosol-facing conformation.

Lying across the cytosolic entrance to the vestibule, the Acidic Helix also coordinates two Ca^{2+} ions (Supplementary Fig. 4c). These two ions lie on the cytosolic side, 11Å from the central Ca^{2+} site, coordinated by Asp234 and Glu230 of the Acidic Helix and by Glu83 of M1 (Fig. 2c). The acidic motif has been suggested to have a role in Ca^{2+} binding[23]. In mammalian NCX members, the analogous region connecting helices M5 and M6 contains a large intracellular calcium-binding domain (CBD1) responsible for stimulating activity in the transporter domain in the presence of Ca^{2+} [28](Supplementary Fig 5). The CBD1 Ca^{2+} binding sites are similarly formed from acidic motifs although they coordinate ions employing β-sheets rather than α-helical secondary structures[29]. Molecular dynamics (MD) simulations performed with the VCX1 structure suggest that the Acidic Helix maintains an α-helical conformation in the presence of the two coordinated Ca^{2+} ions, and becomes more flexible in their absence (Supplementary Fig. 6). The increased rigidity of the VCX1 Acidic Helix at higher Ca^{2+} concentrations indicates a possible Ca^{2+}-dependent regulatory function for this region, perhaps augmenting conductance in the presence of increased cytosolic Ca^{2+}.

Comparison of the two structural repeats (M1-M5 and M6-M10) of VCX1 reveals a structurally similar core region that is closely packed and rigid (M3-M5, M8-M10) (Supplementary Fig. 7b). In contrast, considerable differences are found in the M2a helix and C-terminal half of M1 when compared to M7a and M6. Superposition between helices M1-M2a and M6-M7a reveal a ~12° and 7° asymmetric difference in the angle of M1 and M2a respectively (Supplementary Fig. 7c, 7d). This structural divergence, in combination with loose packing and intracellular location implicate this mobile region as the cytosolic gate. A dynamic straightening of the M1/M2a helices would collapse the cytosolic vestibule,

and this motion could be coordinated by a structural rearrangement into a vacuole-facing conformation.

The VCX1 conformation also sheds light on the transport cycle of CaCA proteins by comparison with the recent structure of an archaebacterial Na^+/Ca^{2+} exchanger from *Methanococcus janaschii* (mjNCX)[17]. Despite low sequence identity (14%) to VCX1, the overall fold and topology of mjNCX is similar. However, unlike VCX1, the mjNCX exchanger is closed to the cytosolic environment and instead represents a periplasm-facing conformation, as reflected in the overall displacement between similar atoms (RMSD 5.7Å over 269 Cα atoms). Structural alignment of the VCX1 and mjNCX structures reveals a similar placement of the core region and of helices M7 and M2b (Supplementary Fig. 8). However, the M2a helix is shifted by ~16Å toward the center of the bilayer in VCX1 (Figure 4a). In addition, relative to the mjNCX structure, the position of both loosely packed helices M1 and M6 are translated diagonally towards the vacuole by ~16Å and ~13Å at either end, closing a vacuole-facing portal that could otherwise expose the active site of the protein to the vacuolar environment (Fig. 4b, Supplementary Fig. 8, 9). The concerted transposition in the M1/M6 helices therefore performs a dual role of coordinating motions between the α-repeats and covering/uncovering an active site entry passage (Fig. 4c). By this mechanism, translational movements of the M1/M6 helices allow alternating access to the active site of VCX1 from both sides of the membrane. The action of the M1/M6 helices is therefore analogous to the piston of a two-stroke engine that occludes and exposes intake and efflux pathways during each turnover. Using a predicted cytosol-facing mjNCX conformation, a similar motion of the M1 and M6 helices was suggested for turnover by the mjNCX monomer[17]. Our data augment the proposed mechanism by including structural evidence for the M1/M6 translations and substantial conformational changes in the M2a helix. With the addition of a cytoplasmic facing VCX1 structure, there are now two key states in the CaCA family that suggest a trajectory for Ca^{2+} translocation, forming a strong case for the two-stroke mechanism of alternating access.

The proposed transport cycle of VCX1 is shown in Figure 4c (Supplementary Video). In the active site, Glu106 and Glu302 are exposed to the vacuolar side (pH ~5-6[30]). The proton motive gradient across the vacuolar membrane provides the source of energy to drive a conformational change to the cytosol-facing conformation whereupon the glutamate residues would be expected to maintain a negative charge (at pH ~7[30]). Under conditions of high cytosolic Ca^{2+} concentration, as seen during signal transduction events, Ca^{2+} is coordinated by the Acidic Helix, and Ca^{2+} is able to reach the active site. The VCX1 side chains of Glu302 and Ser325 partially replace the Ca^{2+} hydration shell, and subsequent completion of coordination by Glu106 displaces some of the remaining water molecules to bring helix M2b inward towards the active site. This movement of M2 towards the core can initiate M2a straightening and M1/M6 translation, closing the cytosolic vestibule. The translation of helices M1/M6 uncovers a vacuolar cleft and coordinates opening of M7a to expose the active site Ca^{2+} ion to the vacuole. The vacuole-facing conformation, in combination with the acidic pH in the vacuole, lowers the Ca^{2+} affinity of active site residues Glu106 and Glu302, leading to release of the Ca^{2+} substrate into the vacuole. The cyclical pumping action of the M1/M6 “piston”, coupled to flexible helices surrounding the active site (M2a,

M7a) provides an efficient framework for the rapid turnover necessary for high throughput Ca^{2+} exchange.

In conclusion, VCX1 is the first CAX family structure, and the first structure of the CaCA superfamily in a cytosol-facing conformation. It provides a structural basis for an alternating access mechanism for the VCX1 protein and the CaCA superfamily in general. These findings lay the groundwork for future exploration of Ca^{2+} transport by CaCA superfamily members and lend insight into fundamental aspects of Ca^{2+} homeostasis and eukaryotic signal transduction processes.

Methods

Expression and purification

The VCX1 protein from *Saccharomyces cerevisiae* (Uniprot ID Q99385) was incorporated into the 2μ expression plasmid p423-GAL1 modified with N-terminal and C-terminal purification-tags as described [31]. Transformed *S. cerevisiae* (strain DSY-5; *MATalpha his3::GAL1-GAL4 pep4 prb1-1122)* were grown in a fermenter culture vessel (Biostat C15L Sartorius AG) to high density and induction was performed via fed-batch using 40% galactose and harvested after 18-22 hours. Harvested yeast (~1.8-2kg wet cell weight) were washed in cold water, pelleted (6000rpm) and flash frozen for storage at -80°C. Frozen pellets were thawed in lysis buffer (100mM Tris 7.0, 700mM NaCl 1mM phenylmethylsulfonyl fluoride (PMSF) + protease inhibitors) before cell disruption using a bead mill. The homogenate was centrifuged for 25 minutes at 21,600g, followed by sedimentation of membranes via ultracentrifugation at 185,000g for 150 minutes. Membrane pellets were resuspended in membrane resuspension buffer (50 mM Tris pH 7.0, 600 mM NaCl, 20% Glycerol) before being frozen in liquid nitrogen in 7g aliquots. 100g cells of yeast cell material yielded an average of 20-25g membrane. Membrane aliquots were thawed and suspended in 112mL membrane solubilisation buffer (50 mM Tris pH 7.0, 600 mM NaCl, 20mM $CaCl_2$, 10% Glycerol 1mM PMSF + protease inhibitors) and solubilized using 1380mg n-dodecyl-beta-D-maltoside (DDM) (1:0.19 (w/w) ratio) for 30 minutes at 4°C, followed by centrifugation at 120,000g for 30min to remove unsolubilized material. The resultant lysate was supplemented with 8mM imidazole pH 6.5 and incubated for ~3hours with 6mL pre-equilibrated TALON Co^{2+} resin. Following incubation, the beads were collected by gravity flow-through using a Bio-Rad econo-column and washed twice via neutation with 30mL buffer A (50mM Tris pH 7.0, 0.1% DDM, 20mM $CaCl_2$, 5mM $MnCl_2$,10% glycerol) supplmented with 15mM and 30mM imidazole pH 6.5 respectively. The protein was eluted from the beads using 3 elutions of 5mL buffer A supplemented by 500mM imidazole pH 6.5). The elutions were pooled, bovine thrombin and 3C protease were added to cleave the tags, and dialyzed with a 25kDa cutoff into 1L of dialysis buffer (50mM MES pH 6.0, 20mM $CaCl_2$, 5mM $MnCl_2$ 10% glycerol) overnight at 4°C. The following day the eluate was concentrated to 500uL and injected onto a size-exclusion column (Superdex 200, GE Healthcare) equilibrated SEC buffer (10mM MES pH 6.0, 0.05% DDM, 20mM $CaCl_2$, 5mM $MnCl_2$). Peak fractions were collected and concentrated to ~30mg/mL. **Reconstitution and transport assay**. Ca^{2+} uptake into proteoliposomes using purified VCX1 protein was performed primarily using the method described by Ridilla

et al[32]. In brief, 10mg of yeast polar lipid extract (Avanti Polar Lipids) was dried under nitrogen and resuspended into 10mM MOPS pH 6.5, 100mM choline chloride, and 100μM Fura-2[33] (Sigma-Aldrich). The resuspension was sonicated to transparency, subjected to 10 cycles of freeze/thaw, and then extruded through a 400nm filter 10 times. The resulting liposomes were destabilized by addition of 1% octyl β-D-glycopyranoside (OG) and purified VCX1 was added in a 1:500 (w/w) ratio and incubated for 1 hour. OG was removed by addition of 200mg/mL Bio-Beads (Bio-Rad) for 3 hours and replaced with 200mg/mL fresh Bio-Beads for incubation overnight. Proteoliposomes were harvested by centrifugation at 66,000g for 150 minutes and resuspended in 10mM MOPS pH 6.5, 100mM choline chloride. Proton gradient was initiated by the addition of 20μl proteoliposome to 20μl reaction buffer containing 100mM choline chloride and 10mM MOPS pH 7.9,7.2 or 6.5 (final pH 7.1, 6.8. 6.5) in a Corning 384 well clear bottom microplate. Transport activity followed the addition of 100μM $CaCl_2$, and uptake of Ca^{2+} was monitored at 22°C via the changes in emission of Fura-2 at 510nm upon excitation at 340 and 380nm at 10 second intervals using a Molecular Devices SpectraMax microplate reader. Maximal signal was obtained via addition of 0.3% DDM, the ratio of emission intensities at the two excitation wavelengths was converted to Ca^{2+} using a standard curve and previously described methods[33]. **Crystallization**. 40μL concentrated VCX1 was mixed with 60μL monoolein to prepare the lipidic cubic phase (LCP) as previously described[34]. Crystals were grown by adding 1μL VCX1/LCP mixture to a glass coverslip and overlayed with 2μL crystallization solution (14% Jeffamine M600 pH 7.0, 100mM Hepes pH 7.0, 50mM $CaCl_2$, 50mM $MnCl_2$, 200mM NaI). Coverslips were sealed in a hanging drop method in 24 well trays containing 300uL crystallization solution. Crystals appeared in a subsequent sponge phase in approximately 3-4 days and grew to a maximum size of 250μm. Crystals were harvested directly from the trays and frozen in liquid nitrogen for data collection. Data was collected at Advanced Light Source beamline 8.3.1, Advanced Photon Source beamline 23-ID-B and Stanford Synchrotron Radiation Lightsource beamline 12-2. Holmium heavy-atom derivatives were obtained by adding $Ho(III)Cl_2$ to the crystals 1 hour prior to flash-cooling, either as salt or as a concentrated, aqueous solution. **Data processing**. Data sets were processed using XDS[35] in space group R3. An initial marginal molecular replacement solution was provided by the mjNCX structure (pdb code 3V5U;14% identity) using the PHENIX[36] AutoMR program and improved upon by PHENIX[36] AutoBuild. Inital Iodine and Holmium heavy atom sites were located in anomalous difference maps calculated in the CCP4[37] package using molecular replacement phases and a holmium derivative dataset. The heavy atom sites were refined using the program AutoSHARP[38], and subsequent density modification was performed using RESOLVE[39]. Refinement of the structure was performed by PHENIX[36] Refine and the model was build using COOT[40]. The assignment of ions in the model was aided by appropriate coordination by liganding side chains and anomalous scattering at Cu Kα wavelength (8keV f"(I^{2-})= 6.9e^-, f"(Mn^{2+})= 2.83e^-, f" (Ca^{2+})=1.3e^-). The final structural model was refined using data to 2.3 Å with a crystallographic R-factor of 20.0% and a free R-factor of 22.4% (Supplementary Table 1). **Comparative modelling and structural analysis**. A comparative model of VCX1 in the vacuole-facing conformation was constructed using MODELLER-9V11[41], based on the mjNCX X-ray structure (PDB identifier 3V5U[17]). The alignment between the sequences of VCX1 and mjNCX was obtained by manually editing the alignments from UCSF Chimera[42] and

PROMALS3D[43]. The VCX1 structure and model was analysed and visualized using UCSF Chimera[42] and PyMol[44], and electrostatic surfaces were calculated using APBS[45]. **MD simulations**. MD simulations were performed with GROMACS4[46], using the CHARMM27[47] all-atom force field and the TIP3P[48] water model. VCX1 was oriented in an implicit lipid bilayer using PPM[49], then immersed in an explicit 1,2-Dimyristoyl-*sn*-Glycero-3-Phosphocholine (DMPC) lipid bilayer and water using CHARMM-GUI[50]. Periodic boundary conditions and a triclinic box with the volume of 604.326 nm^3 were used. Two independent simulations were carried out, one with and another one without the two Ca^{2+} coordinating Glu230 and Asp234. Equilibration was performed by three 10ns long runs, gradually increasing the temperature from 100K to 300K, in the canonical (*NVT*) ensemble controlled by the Berendsen[51] thermostat. The positions of non-hydrogen atoms of VCX1 were restrained by a harmonic potential, with gradually decreasing force constant. A final equilibration step was carried out for 20ns without restraints, in the isothermal–isobaric (*NpT*) ensemble controlled by the semi-isotropic Berendsen51 barostat. Each production run was 100ns long, in the *NpT* ensemble controlled by the Bussi-Donadio-Parrinello[52] thermostat and the semi-isotropic Parrinello-Rahman[53] barostat.

Supplementary Material

Refer to Web version on PubMed Central for supplementary material.

Acknowledgements

We thank James Holton, George Meigs, Craig Ogata, Nagarajan Venugopalan and Tzanko Doukov for assistance with synchrotron data collection at Advanced Light Source, Advanced Photon Source and Stanford Synchrotron Radiation Lightsource; and Christopher Waddling and Pascal Wassam for technical assistance. B.P.P. was supported by a postdoctoral fellowship from the Carlsberg Foundation and later by a fellowship from the Danish Cancer Society; A.S. by NIH grants U54 GM094625 and U01 GM61390; R.M.S. by NIH grants U54 GM094625, GM24485 and GM073210.

References

1. Crespo LM, Grantham CJ, Cannell MB. Kinetics, stoichiometry and role of the Na-Ca exchange mechanism in isolated cardiac myocytes. Nature. 1990; 345:618–621. [PubMed: 2348872]
2. Cui J, et al. Simulating calcium influx and free calcium concentrations in yeast. Cell Calcium. 2009; 45:123–132. [PubMed: 18783827]
3. Miseta A, Kellermayer R, Aiello DP, Fu L, Bedwell DM. The vacuolar Ca2+/H+ exchanger Vcx1p/Hum1p tightly controls cytosolic Ca2+ levels in S. cerevisiae. FEBS Lett. 1999; 451:132–136. [PubMed: 10371152]
4. Philipson KD, Nicoll DA. Sodium-calcium exchange: a molecular perspective. Annu. Rev. Physiol. 2000; 62:111–133. [PubMed: 10845086]
5. Nicoll DA, Longoni S, Philipson KD. Molecular cloning and functional expression of the cardiac sarcolemmal Na(+)-Ca2+ exchanger. Science. 1990; 250:562–565. [PubMed: 1700476]
6. Lytton J. Na+/Ca2+ exchangers: three mammalian gene families control Ca2+ transport. Biochem. J. 2007; 406:365–382. [PubMed: 17716241]
7. Hirschi KD, Zhen RG, Cunningham KW, Rea PA, Fink GR. CAX1, an H+/Ca2+ antiporter from Arabidopsis. Proc. Natl. Acad. Sci. U.S.A. 1996; 93:8782–8786. [PubMed: 8710949]
8. Pozos TC, Sekler I, Cyert MS. The product of HUM1, a novel yeast gene, is required for vacuolar Ca2+/H+ exchange and is related to mammalian Na+/Ca2+ exchangers. Mol. Cell. Biol. 1996; 16:3730–3741. [PubMed: 8668190]

9. Cheng N-H, Pittman JK, Barkla BJ, Shigaki T, Hirschi KD. The Arabidopsis cax1 mutant exhibits impaired ion homeostasis, development, and hormonal responses and reveals interplay among vacuolar transporters. Plant Cell. 2003; 15:347–364. [PubMed: 12566577]
10. Cho D, et al. Vacuolar CAX1 and CAX3 influence auxin transport in guard cells via regulation of apoplastic pH. Plant Physiol. 2012 doi:10.1104/pp.112.201442.
11. Cunningham KW. Acidic calcium stores of Saccharomyces cerevisiae. Cell Calcium. 2011; 50:129–138. [PubMed: 21377728]
12. Shigaki T, Rees I, Nakhleh L, Hirschi KD. Identification of three distinct phylogenetic groups of CAX cation/proton antiporters. J. Mol. Evol. 2006; 63:815–825. [PubMed: 17086450]
13. Denis V, Cyert MS. Internal Ca(2+) release in yeast is triggered by hypertonic shock and mediated by a TRP channel homologue. J. Cell Biol. 2002; 156:29–34. [PubMed: 11781332]
14. Schwarz EM, Benzer S. Calx, a Na-Ca exchanger gene of Drosophila melanogaster. Proc. Natl. Acad. Sci. U.S.A. 1997; 94:10249–10254. [PubMed: 9294196]
15. Cai X, Lytton J. The cation/Ca(2+) exchanger superfamily: phylogenetic analysis and structural implications. Mol. Biol. Evol. 2004; 21:1692–1703. [PubMed: 15163769]
16. Iwamoto T, et al. Unique topology of the internal repeats in the cardiac Na+/Ca2+ exchanger. FEBS Lett. 1999; 446:264–268. [PubMed: 10100855]
17. Liao J, et al. Structural insight into the ion-exchange mechanism of the sodium/calcium exchanger. Science. 2012; 335:686–690. [PubMed: 22323814]
18. Nicoll DA, Hryshko LV, Matsuoka S, Frank JS, Philipson KD. Mutation of amino acid residues in the putative transmembrane segments of the cardiac sarcolemmal Na+-Ca2+ exchanger. J. Biol. Chem. 1996; 271:13385–13391. [PubMed: 8662775]
19. Winkfein RJ, et al. Scanning Mutagenesis of the Alpha Repeats and of the Transmembrane Acidic Residues of the Human Retinal Cone Na/Ca-K Exchanger†. Biochemistry. 2003; 42:543–552. [PubMed: 12525183]
20. Kang K-J. Residues Contributing to the Ca2+ and K+ Binding Pocket of the NCKX2 Na+/Ca2+-K + Exchanger. Journal of Biological Chemistry. 2005; 280:6823–6833. [PubMed: 15583008]
21. Pittman JK, Sreevidya CS, Shigaki T, Ueoka-Nakanishi H, Hirschi KD. Distinct N-terminal regulatory domains of Ca(2+)/H(+) antiporters. Plant Physiol. 2002; 130:1054–1062. [PubMed: 12376668]
22. Pittman JK, Hirschi KD. Regulation of CAX1, an Arabidopsis Ca(2+)/H+ antiporter. Identification of an N-terminal autoinhibitory domain. Plant Physiol. 2001; 127:1020–1029. [PubMed: 11706183]
23. Ivey DM, et al. Cloning and characterization of a putative Ca2+/H+ antiporter gene from Escherichia coli upon functional complementation of Na+/H+ antiporter-deficient strains by the overexpressed gene. J. Biol. Chem. 1993; 268:11296–11303. [PubMed: 8496184]
24. Ohsumi Y, Anraku Y. Calcium transport driven by a proton motive force in vacuolar membrane vesicles of Saccharomyces cerevisiae. J. Biol. Chem. 1983; 258:5614–5617. [PubMed: 6343390]
25. Dunn T, Gable K, Beeler T. Regulation of cellular Ca2+ by yeast vacuoles. J. Biol. Chem. 1994; 269:7273–7278. [PubMed: 8125940]
26. Kamiya T, Maeshima M. Residues in internal repeats of the rice cation/H+ exchanger are involved in the transport and selection of cations. J. Biol. Chem. 2004; 279:812–819. [PubMed: 14561741]
27. Shigaki T, et al. Identification of a crucial histidine involved in metal transport activity in the Arabidopsis cation/H+ exchanger CAX1. J. Biol. Chem. 2005; 280:30136–30142. [PubMed: 15994298]
28. Matsuoka S, Nicoll DA, Reilly RF, Hilgemann DW, Philipson KD. Initial localization of regulatory regions of the cardiac sarcolemmal Na(+)-Ca2+ exchanger. Proc. Natl. Acad. Sci. U.S.A. 1993; 90:3870–3874. [PubMed: 8483905]
29. Nicoll DA, et al. The crystal structure of the primary Ca2+ sensor of the Na+/Ca2+ exchanger reveals a novel Ca2+ binding motif. J. Biol. Chem. 2006; 281:21577–21581. [PubMed: 16774926]
30. Martínez-Muñoz GA, Kane P. Vacuolar and plasma membrane proton pumps collaborate to achieve cytosolic pH homeostasis in yeast. J. Biol. Chem. 2008; 283:20309–20319. [PubMed: 18502746]

31. Li M, et al. Selecting Optimum Eukaryotic Integral Membrane Proteins for Structure Determination by Rapid Expression and Solubilization Screening. Journal of Molecular Biology. 2009; 385:820–830. [PubMed: 19061901]
32. Ridilla M, Narayanan A, Bolin JT, Yernool DA. Identification of the Dimer Interface of a Bacterial Ca(2+)/H(+) Antiporter. Biochemistry. 2012 doi:10.1021/bi3012109.
33. Grynkiewicz G, Poenie M, Tsien RY. A new generation of Ca2+ indicators with greatly improved fluorescence properties. J. Biol. Chem. 1985; 260:3440–3450. [PubMed: 3838314]
34. Caffrey M, Cherezov V. Crystallizing membrane proteins using lipidic mesophases. Nature Protocols. 2009; 4:706–731. [PubMed: 19390528]
35. Kabsch W. XDS. Acta Crystallogr. D Biol. Crystallogr. 2010; 66:125–132. [PubMed: 20124692]
36. Adams PD, et al. PHENIX : a comprehensive Python-based system for macromolecular structure solution. Acta Crystallographica Section D Biological Crystallography. 2010; 66:213–221.
37. Winn MD, et al. Overview of the CCP4 suite and current developments. Acta Crystallogr. D Biol. Crystallogr. 2011; 67:235–242. [PubMed: 21460441]
38. Vonrhein C, Blanc E, Roversi P, Bricogne G. Automated structure solution with autoSHARP. Methods Mol. Biol. 2007; 364:215–230. [PubMed: 17172768]
39. Terwilliger TC. Maximum-likelihood density modification. Acta Crystallogr. D Biol. Crystallogr. 2000; 56:965–972. [PubMed: 10944333]
40. Emsley P, Cowtan K. Coot: model-building tools for molecular graphics. Acta Crystallogr. D Biol. Crystallogr. 2004; 60:2126–2132. [PubMed: 15572765]
41. Sali A, Blundell TL. Comparative protein modelling by satisfaction of spatial restraints. J. Mol. Biol. 1993; 234:779–815. [PubMed: 8254673]
42. Pettersen EF, et al. UCSF Chimera--a visualization system for exploratory research and analysis. J Comput Chem. 2004; 25:1605–1612. [PubMed: 15264254]
43. Pei J, Kim B-H, Grishin NV. PROMALS3D: a tool for multiple protein sequence and structure alignments. Nucleic Acids Res. 2008; 36:2295–2300. [PubMed: 18287115]
44. The PyMOL Molecular Graphics System. Version 1.5.0.4 Schrödinger. LLC;
45. Baker NA, Sept D, Joseph S, Holst MJ, McCammon JA. Electrostatics of nanosystems: Application to microtubules and the ribosome. PNAS. 2001; 98:10037–10041. [PubMed: 11517324]
46. Hess B, Kutzner C, Van der Spoel D, Lindahl E. GROMACS 4: Algorithms for Highly Efficient, Load-Balanced, and Scalable Molecular Simulation. J. Chem. Theory Comput. 2008; 4:435–447. [PubMed: 26620784]
47. Bjelkmar P, Larsson P, Cuendet MA, Hess B, Lindahl E. Implementation of the CHARMM Force Field in GROMACS: Analysis of Protein Stability Effects from Correction Maps, Virtual Interaction Sites, and Water Models. J. Chem. Theory Comput. 2010; 6:459–466. [PubMed: 26617301]
48. Jorgensen WL, Chandrasekhar J, Madura JD, Impey RW, Klein ML. Comparison of simple potential functions for simulating liquid water. The Journal of Chemical Physics. 1983; 79:926–935.
49. Lomize MA, Pogozheva ID, Joo H, Mosberg HI, Lomize AL. OPM database and PPM web server: resources for positioning of proteins in membranes. Nucleic Acids Res. 2012; 40:D370–376. [PubMed: 21890895]
50. Jo S, Lim JB, Klauda JB, Im W. CHARMM-GUI Membrane Builder for mixed bilayers and its application to yeast membranes. Biophys. J. 2009; 97:50–58. [PubMed: 19580743]
51. Berendsen HJC, Postma JPM, Van Gunsteren WF, DiNola A, Haak JR. Molecular dynamics with coupling to an external bath. The Journal of Chemical Physics. 1984; 81:3684–3690.
52. Bussi G, Donadio D, Parrinello M. Canonical sampling through velocity rescaling. The Journal of Chemical Physics. 2007; 126:014101–014101–7. [PubMed: 17212484]
53. Parrinello M, Rahman A. Polymorphic transitions in single crystals: A new molecular dynamics method. Journal of Applied Physics. 1981; 52:7182–7190.

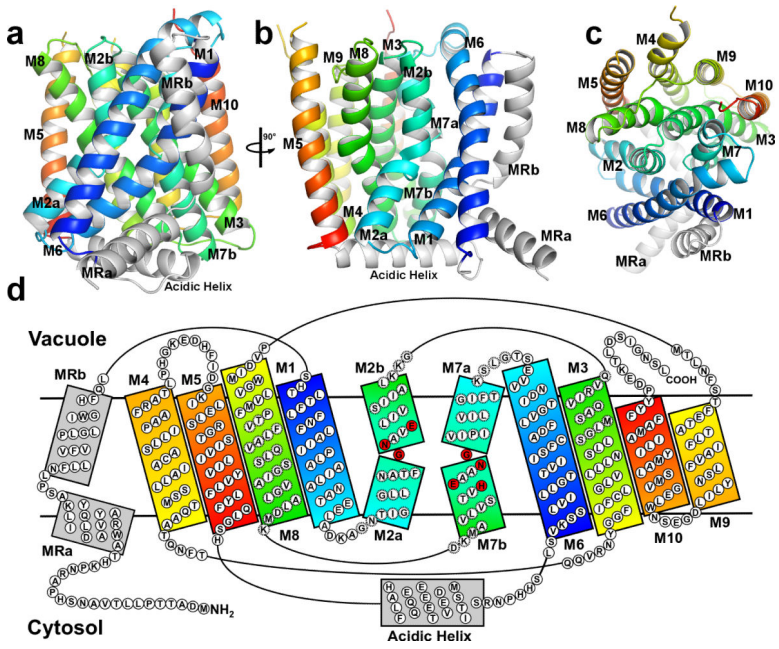

Figure 1. Topology and fold of the VCX1 protein

The symmetrically related halves of the VCX1 monomer are colored in a double rainbow from the N to C terminus. Helices of matching color are related by symmetry. **a**, The VCX1 monomer as viewed in the membrane along the axis of symmetry, **b**, rotated by 90° and **c**, viewed from the vacuolar side of the membrane. **d**, Topology map of the VCX1 monomer; CAX family conserved residues are colored in red, α-repeat sequences are denoted by dashed circles.

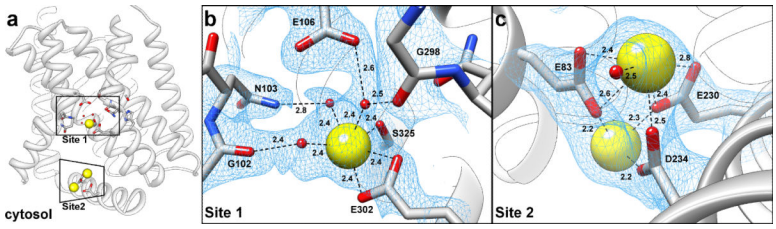

Figure 2. Calcium binding sites in the VCX1 crystal structure

a, Overview of Site 1 and Site 2 with helices MR, M1, and M6 removed for clarity. The cytosol is on the bottom of the image and Ca^{2+} ions are colored in yellow. **b**, Active site Ca^{2+} substrate ion and interacting residues found in Site 1. Hydrogen bonds are shown as dashed lines; numbers denote atomic distances (Å). 2mFo-DFc map is shown contoured at 1σ (blue mesh) **c**, Ca^{2+} ions at the Acidic Helix, in Site 2 with interacting residues labeled. Hydrogen bonds are shown as dashed lines; numbers denote atomic distances (Å). 2mFo-DFc map is shown contoured at 1σ (blue mesh)

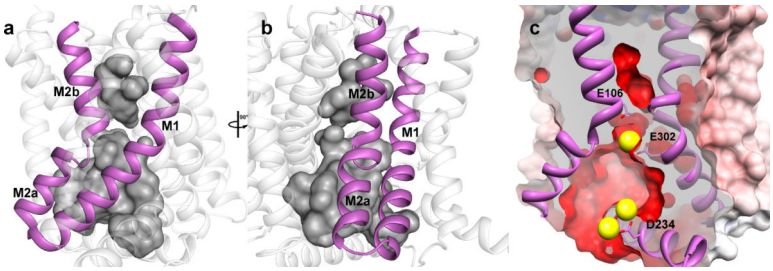

Figure 3. The cytoplasmic vestibule

a, The protein cavity is rendered as a surface and colored in grey, the helices M1 and M2 are colored in purple and shown from the axis of symmetry. **b**, View rotated by 90°. **c**, The cytoplasmic vestibule as oriented in panel **a** and depicted with a slab surface representation colored by electrostatic potential (red to blue; -10 to 10kT/e). Helices MR, M1 and M6 have been removed for clarity. Ca^{2+} ions (yellow spheres) pinpoint Site 1 and Site 2.

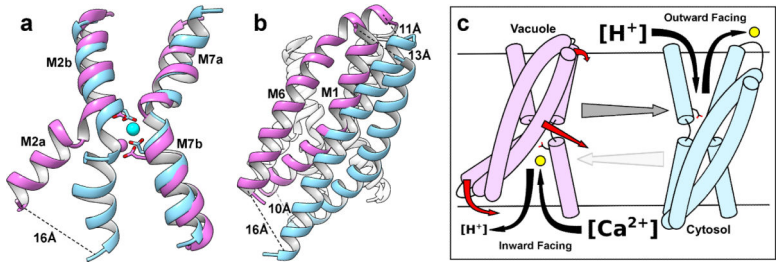

Figure 4. Transport cycle of VCX1 and structural comparison to mjNCX

a, Comparison of M2 and M7 and active site glutamate residues between VCX1 (purple) and mjNCX (cyan). Ca^{2+} ions from each model are depicted as spheres. **b**, Comparison of M1 and M6 between VCX1 (purple) and mjNCX (cyan). **c**, Schematic of VCX1 turnover. Structures are colored as in panel **a**. Proposed substrate movement is denoted by black arrows, and calcium by yellow circles. Red arrows show protein movement in the cytosol-facing facing state of VCX1 (left) that results in the vacuole-facing conformation on the right. Return to the cytosol-facing state presumably requires reversal of the movements denoted by the red arrows.